RSC Advances



This is an *Accepted Manuscript*, which has been through the Royal Society of Chemistry peer review process and has been accepted for publication.

Accepted Manuscripts are published online shortly after acceptance, before technical editing, formatting and proof reading. Using this free service, authors can make their results available to the community, in citable form, before we publish the edited article. This Accepted Manuscript will be replaced by the edited, formatted and paginated article as soon as this is available.

You can find more information about *Accepted Manuscripts* in the **Information for Authors**.

Please note that technical editing may introduce minor changes to the text and/or graphics, which may alter content. The journal's standard <u>Terms & Conditions</u> and the <u>Ethical guidelines</u> still apply. In no event shall the Royal Society of Chemistry be held responsible for any errors or omissions in this *Accepted Manuscript* or any consequences arising from the use of any information it contains.



Cite this: DOI: 10.1039/c0xx00000x

www.rsc.org/xxxxxx

ARTICLE TYPE

Activated clay of roost structure encapsulated sulfur cathodes for lithium-sulfur batteries

Zhaoxia Cao, ^{a,b,c} Chao Ma, ^{a,b,c} Yujie Jia, ^{a,b,c} Zhixian Sun, ^{a,b,c} Hongyun Yue, ^{a,b,c} Yanhong Yin, ^{a,b,c} Shuting Yang *a,b,c</sup>

s Received (in XXX, XXX) XthXXXXXXXX 20XX, Accepted Xth XXXXXXXX 20XX DOI: 10.1039/b000000x

Activated clay (AC) of roost structure with large surface area is employed to support sulfur for the cathode of lithium sulfur battery. The special structure may take a similar effect like the small filter screens for entrapping sulfur and restricting the diffusion of the polysulfides during cycling. A high capacity of 959.6 mA h g⁻¹ achieves at a rate of 0.1 C in the first cycle for the AC/S with sulfur content of 57 wt% and the reversible capacity remains high at up to 700.9 mA h g⁻¹ even after 50 cycles.

1. Introduction

Lithium-sulfur (Li-S) batteries are one of the prospective candidates in this regard, as sulfur offers high theoretical specific capacity of 1675 mA h g⁻¹ at a safe operating voltage and low cost. However, although this system has been attracting attention for more than two decades, it has not been commercialized on a large scale due to several unsolved problems, such as the inherent poor electrical conductivity of S (5 to × 10⁻³⁰ S cm⁻¹ at 25 °C), and a poor cycling performance caused by high electrolyte-soluble lithium polysulfide intermediates formed during the repeated discharge-charge processes so on. To overcome these problems effectively, studies of the well-designed cathode of Li-S batteries are of great importance. However, and the prospective capacity of the series of the self-designed cathode of Li-S batteries are of great importance.

25 In recent years, sulfur is always combined with porous substrates through proper structure design (surface coating and/or sulfur loading) to effectively confine sulfur on the cathode side and limit dissolution of polysulfides in the electrolyte. These substrates include of porous carbons/polymers/metal oxides and 30 functionalized graphenes that limit polysulfides dissolution through both physical and chemical interactions.⁸⁻¹⁹ Here, we propose to use clays as confined substrate for sulfur impregnation. Clays (Al₂O₃•4SiO₂•nH₂O), are very common in the natural environment, non-toxic and lower-cost. They play a 35 vital role in terrestrial biogeochemical cycles and containment of toxic waste materials.²⁰ As a result of their high surface area and abundant surface functional groups, they have been discovered to have good catalytic/support properties, especially for many organic reactions and bleaching purposes. With its large pore 40 volume and small windows limiting the diffusion processes, this material appears as a suitable candidate for the encapsulation of

sulfur and its corresponding reduced state species inspite of their low electric conductivities. The confinement effect of a porous

material is more important than its conductivity for Li-S

electrodes can be improved by using enough Super P to build a

45 batteries. 21 Furthermore, the overall electronic conductivity of the

conductive network.²² So, activated clay (AC) with a threedimensional roost structure has been employed to design a novel composite of sulfur/activated clay (Fig. 1). After simple acidification treatment, the clays are exfoliated into desultorily and unsystematic nanorods which look like a roost. Compared with traditional sulfur cathode materials, the sulfur/activated clay (AC/S) composite with special structure has several advantages.

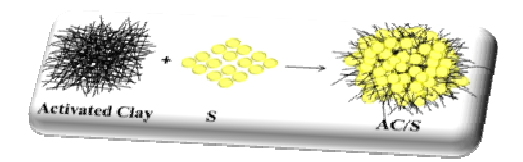


Fig. 1 Scheme of the sulfur/activated clay (AC) composite

Firstly, the roost-like structure can provide more active sites and reduce the loss of active materials due to its high pecific surface area. Most of the embedded sulfur is located in micropores or under the filter screen through capillary action and filtraltion, which makes the sulfur interact with the oxide nanorods intensively. Secondly, besides the confinement effect, the surface activity of the AC appears to also have a pronounced effect of reducing lithium polysulfide dissolution, and tremendously alleviate the shuttle effect. In addition, the composite can also accommodate the volume expansion of sulfur generated during the electrochemical reaction. At last, the roost structure in the composite is designed to retain pathways for the mass transport of Li ions and endow the cathode a high ionic conductivity.

2. Experimental

70 2.1 Material preparation

The clays were combed out the impurities by HCl and distilled water and dried at 120 °C for 24 h in vacuum drying oven. The as-prepared activated clay mixture of clay (AC) was thoroughly mixed with sublimed sulfur in an agate mortar at different mass

ratios. The mixture was then sealed in an air-free glass container and heated at 155 °C for 6 h to obtain sulfur/activated clay composite (AC/S).

2.2 Material Characterization

⁵ The sulfur content of the composites was confirmed using a thermogravimetric analyzer (TG, STA 449 F3, NETZSCH). The microstructure and morphology of AC and AC/S composites were detected using Brunauer-Emmet-Teller method (BET, Tristar-II, Micromeritics), X-ray diffraction (XRD, Bruker AXS D8), transmission electron microscopy (TEM, JEM-2100, JEOL), and field emission scanning electron microscopy (FE-SEM, SU-8010, HITACHI).

2.3 Electrochemical measurements

In order to prepare the working electrode, the AC/S working electrodes were made by mixing 70 wt% the active material, 20 wt% Super P and 10 wt% PVDF with N-methyl-2-pyrrolidine (NMP). Lithium metal was used as counter and Celgard 2400 was used as the separator. The electrolyte used was 1 M LITFSI in a mixture of Dimethoxyethane (DME) and 1, 3-Dioxolane (DOL) ²⁰ (2:1 volume).

Galvanostatic charge-discharge experiment data were collected using LAND Cell test system (CT2001A, Wuhan, China). The AC impedance measurements and CV (cyclic voltammetry) were carried out using an electrochemical workstation (CHI660B, 25 Shanghai, China).

3. Results and discussion

The content of sulfur in AC/S composites is measured by thermogravimetric analysis (TG) under N_2 atmosphere as shown in Fig. 2. The weight loss of the composite can be observed with increasing temperature from about 150 °C, and the curve become stable when the composite is heated over 350 °C due to evaporation of sulfur from the substrate material of AC. The sulfur content in the as-prepared composite are 63 wt%, 57 wt% and 41 wt%, respectively, in comparision with sublimed sulfur, 35 calculated from the TG curves.

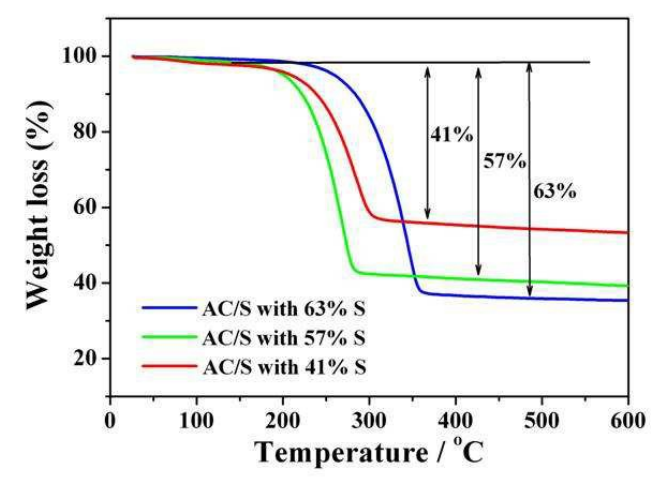
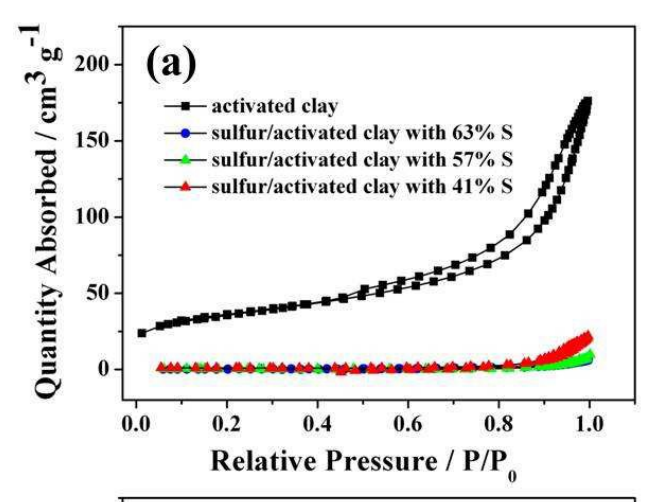


Fig. 2 TG curve of the AC/S composite recorded under N_2 atmosphere.

Tab. 1 Specific surface area and pore volume of the AC and AC/S composite.

Samples	S_{BET} (m ² g ⁻¹)	V _{micro} (cm ³ g ⁻¹)	$V_t (cm^3 g^{-1})$
AC	122.01	0.0133	0.2565
AC/S with 41% S	2.66	0.0023	0.0338
AC/S with 57% S	1.34	0.0006	0.0122
AC/S with 63% S	0.95	< 0.0001	0.0096

40 S_{BET} is the specific surface area, and V_t is the total pore volume.



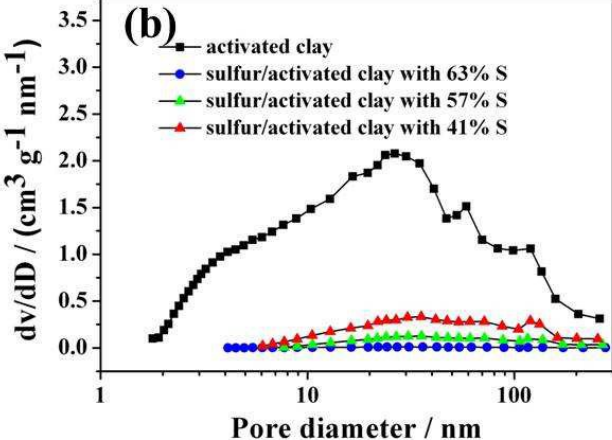


Fig. 3 a) N_2 sorption isotherm and b) pore size distribution of the AC, AC/S with 63 wt%, 57 wt% and 41 wt% sulfur composite.

In order to prove the existence of hierarchical porous structure of the AC substrate, we measured the nitrogen adsorption—desorption isotherm (Fig. 3a) at 77 K and the corresponding density functional theory pore size distribution curve (Fig. 3b). From Fig. 3, we should be able to prove the above conclusion.

The general shape of the isotherm is defined as type III according to IUPAC and suggests the existence of pore sizes ranging from micro- to macropores. The slow increase at a relatively low pressure of P/P₀ (0.01-0.1) reveals the existence of few micropores. The following slope at medium relative pressure and the hysteresisloop in the adsorption–desorption isotherm (as type 55 H3 according to IUPAC) illustrate the presence of developed mesoporosity, while the final abrupt increased tail at the relative pressure from 0.9 to 1.0 indicates the existence of seam type pores. The AC substrate has a pore size distribution mainly in three regions: 1.79-2.0 nm, 2.13-47 nm and > 100 nm, 60 representing three level small micropores, abundant mesopores

45

and a bit of macropores. The Brunauer–Emmett–Teller (BET) surface area of AC reduced dramatically from 122.01 m² g⁻¹ to 2.66 m² g⁻¹, 1.34 m² g⁻¹ and 0.95 m² g⁻¹ after loading different sulfur content, and the total pore volume reduced from 0.2565 5 cm³ g⁻¹ to 0.0338 cm³ g⁻¹, 0.0122 cm³ g⁻¹ and 0.0096 cm³ g⁻¹ (Tab. 1).

The morphology and structure of the AC and the prepared AC/S composite are characterized by FE-SEM and TEM in Fig. 4. Tens of thousands of nanorods cluster into one large particle which 10 looks like the roost structure. That special structure may take a similar effect like the small filter screens (Fig. 4a and c). As shown in Fig. 4b, the roost structure is less obvious due to overlayed by sulfur. Evidence of S containment and the identification of an imbedded entrapped sulfur structure within 15 the AC/S composite are provided by TEM images (Fig. 4c, d) and XRD (Fig. 5a), respectively. Fig. 4d shows the corresponding high resolution TEM (HRTEM) images of the AC/S composite. The dispersed S at its crystalline state was around 0.38 nm with d-spacing (222). Fig. 5a shows the XRD patterns of the pristine 20 sulfur powders and the as-prepared AC/S composite. All diffraction peaks of sulfur match very well with the standard diffraction lines of sulfur (JCPDS card NO. 08-0247), reviewing that the as entrapped sulfur microparticle can be indexed to orthorhombic crystal type. These XRD results are in good 25 agreement with TEM. Fig. 5b is the FTIR spectra of AC, S and AC/S. After sulfur impregnation, two peaks at 465 and 438 cm⁻¹ are observed of AC/S, which is different from that of pristine AC with only a broad one. The weak absorption at 465 cm⁻¹ could be undoubtedly assigned to the S-S vibration mode of elemental 30 sulfur (S₈), while the newly emerged peak at 438 cm⁻¹ could be explained by the weak interaction between sulfur and activated clay.

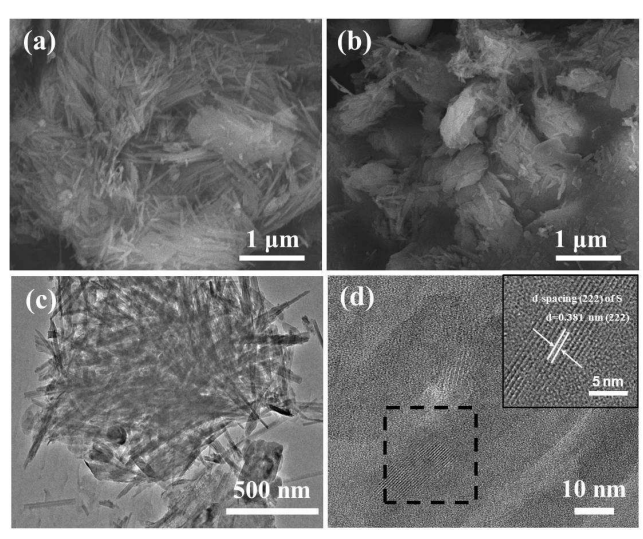


Fig. 4 FESEM images of (a) the activated clay and (b) the AC/S with 57 wt% sulfur composite. And TEM images of (c) the activated clay and (d) AC/S with 57 wt% sulfur composite.

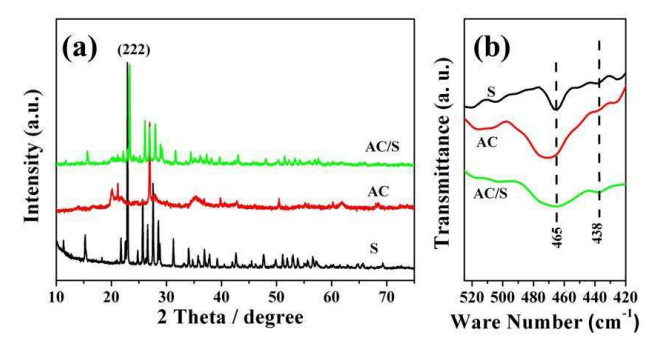


Fig. 5 a) X-ray diffraction patterns of S, AC and AC/S, and b) FTIR spectra of S, AC and AC/S ranging from 420 -520 cm⁻¹.

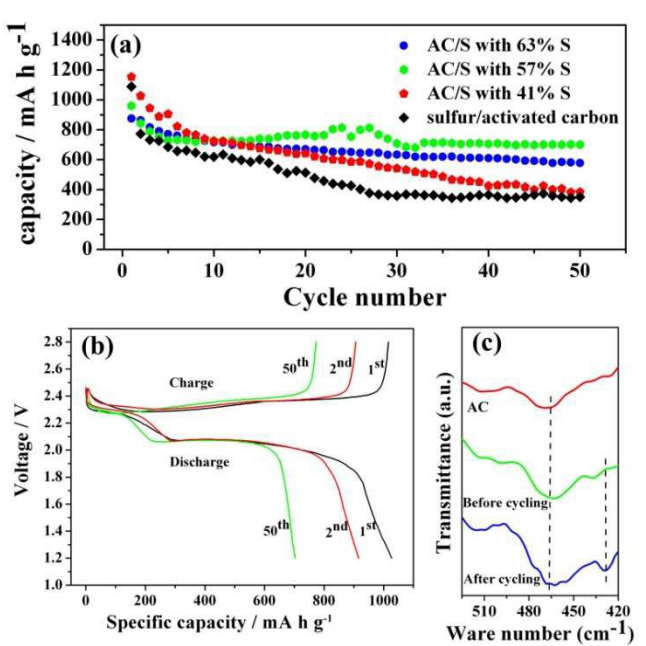


Fig. 6 a) Cycling stability of AC/S with sulfur content of 63 wt%, 57 wt% and 41 wt% at a rate of 0.1 C at a voltage range of 1.2-2.8 V, b) Charge-discharge curves in different cycling numbers of AC/S with 57 wt% sulfur at a rate of 0.1 C, c) FTIR spectra of AC, AC/S before and after cycling ranging from 420 -520 cm⁻¹.

Electrochemical performance of the AC/S composite was investigated using galvanostatic charge/discharge measurements. The C rate specified in this study is based on the mass and theoretical capacity of sulfur (1 C = 1675 mA g^{-1}). The discharge 50 capacity of the AC/S composite was shown in Fig. 6a. The AC/S composite with 57 wt% S shows a high capacity of 959.6 mA h g ¹ at a rate of 0.1 C in the first cycle and the reversible capacity remains high at up to 700.9 mA h g⁻¹ even after 50 cycles. The capacity of AC/S composite with 57 wt% S falls at the first ten 55 cycles then rising gradually due to the slow kinetics. Also, the AC/S composite with 63 wt% S gives a similar trendency with a slightly lower capacity. In contrast, the capacity of AC/S composite with 41 wt% S drops rapidly even it has the largest initial capacity. The initial capacity is closely related to the 60 amount of sulfur loading. A higher sulfur content results in a lower initial capacity, and lower sulfur content results in a poor cycling stability, which are in agreement with previous findings using bimodal pore structure carbon for sulfur impregnation.²³ The rapid initial capacity loss is also observed in the

sulfur/activated carbon composite. When both capacity and cycling stability are considered, he AC/S composite with 57 wt% S exhibits the best electrochemical performance. Although active clays and sufur both have poor conducting nature, the initial 5 discharge capacity is comparable to that delivered by usual C/S composite, as seen in this case. It proves that the AC can provide a special and stable structure for the sulfur entrapment, which is indicative of the greater importance of electrode confinement over electrode conductivity in some case. It also manifests that 10 the overall electronic conductivity of the sulfur cathode can be effectively improved using enough Super P to form a conductive network. The excellent cycling stability may be owing to the special structure of the AC/S composite. The special structure of the composite can restrict the diffusion of polysulfides during the 15 charge/discharge process. In addition, AC can present more polarized surfaces than carbon so that they are capable to interact strongly with charged species, such as Li₂S_x. Thus, one would expect the onset of such surface interactions between the host structures and polysulfides to slow down the migration of the 20 polysulfide species. Hence, the better capacity retention of composite electrodes is what we experimentally observed.

Fig. 6b presents typical discharge/charge profiles of AC/S composite with 57 wt% S for the first, second and fiftieth cycles at a rate of 0.1 C between 1.2-2.8 V. There are two plateaus. One 25 short higher potential plateau at about 2.3 V and another prolonged lower potential plateau at about 2.0 V are presented in the discharge profile. The charge/discharge curves are well maintained during extended cycling. To explore the effect of this special structure during the charging/discharging processes, the 30 FTIR test of the AC/S composite after charging/discharging process is conducted. As shown in Fig. 6c, the newly emerged peak around 438 cm⁻¹ compared with pristine AC which explained by the weak interaction between sulfur and activated clay also appears with a slight blue shift after 50 cycles. The 35 result indicates that the roost-like structure favors the confinement of sulfur and imparts the excellent cell performance in the cycling.

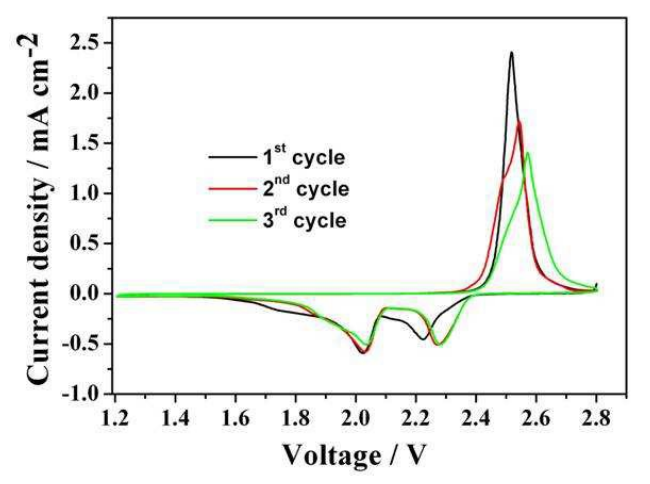


Fig. 7 Cyclic voltammograms of AC/S composite with 57 wt% S at a sweep rate of 0.05 mV s⁻¹

Fig. 7 shows the cyclic voltammograms of the cell for the first three cycles. In the initial cathodic process, two broad reduction peaks appearing at 2.0 and 2.25 V (vs. Li/Li⁺), respectively, is

due to the two-step reduction of sulfur with metallic lithium. In the following cycles, the cathodic peak potentials move up to about 2.05 and 2.3 V (vs. Li/Li⁺), which is ascribed to the polarization of the electrode in the first cycle. In particular, the cathodic peak areas remain almost unchanged, and the anodic peaks have a slight negative shift, which confirms a relatively 50 good reversibility and stability after the initial electrochemical process for AC/S electrode. 24, 25

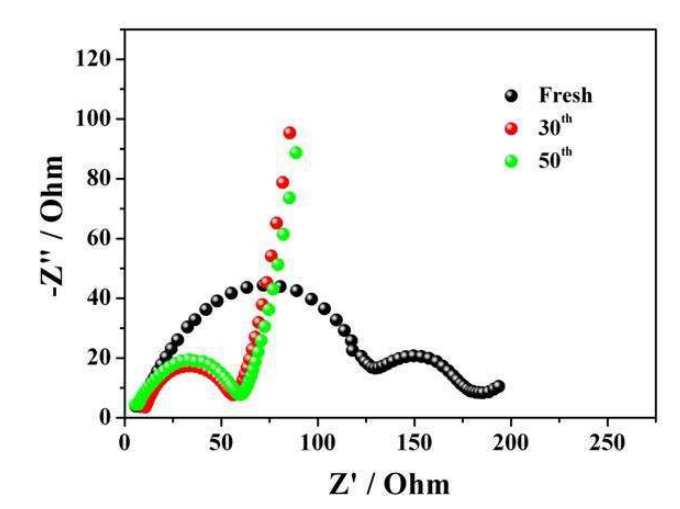


Fig. 8 EIS spectra of AC/S composite with 57 wt% S.

For further analyze the attenuation mechanism of AC/S 55 composite electrode, the electrochemical impedance spectroscopy (EIS) is displayed in Fig. 8. The impedance behaviors of the composite without electrochemical activation are very different from that of the composite experiencing many cycles. The former is composed of two semicircles at high frequency and a nearly 60 straight line at low frequency, while at high frequency, the latter has only one semicircle. As we know, the semi-circle in the high to medium frequency region relates to the resistances of charge transfer and the SEI film, the oblique straight line in the low frequency region corresponds to the diffusion process within the 65 cathodes. It is obvious that the AC/S composite electrode exhibited a low and stable charge transfer resistance upon cycling. The decreased resistance of the AC/S composite electrode along with cycling may be due to that roost-like clay can chemically or physically adsorb polysulfide anions partially restrained the 70 migration of polysulfide.

4. Conclusions

In summary, the roost structure of activated clay with numerous mesoporous and microporou pores has been discovered to improve the electrochemical performance of the Li-S battery. The special roost structure may take a similar effect like the small filter screens for entrapping sulfur and restricting the diffusion of the polysulfides during cycling. Our test results indicate that once sulfur is loaded within the porous framework with a proper ratio of AC/S, the poor cycle stability issue of the sulfur electrode can be partially mitigate because of the confinement effect of the porous frame-work.

Acknowledgement

This work was financially supported by Foundation of He'nan Educational Committee (15A150012).

Notes and references

- ^a School of Chemistry and Chemical Engineering, Henan Normal
- 5 University, Xinxiang Henan 453007, P. R. China.
- $E-mail: \underline{shutingyang@foxmail.com}; Fax: (+86)-373-3326439; Tel: (+86)-373-3326439$
- ^b Engineering Technology Research Center of Motive Power and Key Materials of Henan Province, Xinxiang Henan 453007, P. R. China
- ^c Collaborative Innovation Center of Henan Province for Green Motive Power and Key Materials, Henan Normal University, Xinxiang Henan 453007, P. R. China
 - † Electronic Supplementary Information (ESI) available: See DOI: 10.1039/b000000x/
- 15 ‡ Footnotes should appear here. These might include comments relevant to but not central to the matter under discussion, limited experimental and spectral data, and crystallographic data.
 - W. Wei, J. L. Wang, L. J. Zhou, J. Yang, B. Schumann and Y. N. NuLi, Electrochemistry Communications, 2011, 13, 399.
- 20 2 P. G. Bruce, S. A. Freunberger, L. J. Hardwick and J. M. Tarascon, Nature materials, 2012, 11, 19.
 - 3 K. T. L. Xiulei Ji, Linda F. Nazar, Nature materials, 2009, 8, 500.
 - 4 B. C. Duan, W. K. Wang, A. B. Wang, Z. B. Yu, H. L. Zhao and Y. S. Yang, *Journal Of Materials Chemistry A*, 2014, **2**, 308.
- 25 5 S. Evers and L. F. Nazar, Accounts Chem Res, 2013, 46, 1135.
 - 6 H. Kim, H. D. Lim, J. Kim and K. Kang, *Journal Of Materials Chemistry A*, 2014, **2**, 33.
 - A. Manthiram, Y. Z. Fu and Y. S. Su, Accounts Chem Res, 2013, 46, 1125.
- 30 8 A. Manthiram, Y. Fu and Y. S. Su, Acc Chem Res, 2013, 46, 1125.
- 9 M. M. Rao, W. S. Li and E. J. Cairns, *Electrochemistry Communications*, 2012, 17, 1.
- 10 B. Zhang, X. Qin, G. R. Li and X. P. Gao, Energy & Environmental Science, 2010, 3, 1531.
- 35 11 L. Ji, M. Rao, H. Zheng, L. Zhang, Y. Li, W. Duan, J. Guo, E. J. Cairns and Y. Zhang, Journal of the American Chemical Society, 2011, 133, 18522.
 - 12 D. Wang, Q. Zeng, G. Zhou, L. Yin, F. Li, H. Cheng, I. R. Gentle and G. Q. M. Lu, *Journal of Materials Chemistry A*, 2013, 1, 9382.
- 40 13 G. Zheng, Y. Yang, J. J. Cha, S. S. Hong and Y. Cui, *Nano letters*, 2011, 11, 4462.
 - 14 E. Frackowiak, Physical chemistry chemical physics, 2007, 9, 1774.
 - 15 L. Ji, M. Rao, S. Aloni, L. Wang, E. J. Cairns and Y. Zhang, Energy & Environmental Science, 2011, 4, 5053.
- 45 16 S. Dorfler, M. Hagen, H. Althues, J. Tubke, S. Kaskel and M. J. Hoffmann, Chem Commun (Camb), 2012, 48, 4097.
 - 17 J. Guo, Y. Xu and C. Wang, Nano letters, 2011, 11, 4288.
- 18 J. Schuster, G. He, B. Mandlmeier, T. Yim, K. T. Lee, T. Bein and L. F. Nazar, Angew Chem Int Ed Engl, 2012, 51, 3591.
- 50 19 Y. Yin, C. Ma, Z. Cao, Z. Sun, Y. Jia and S. Yang, RSC Advances, 2014, 4, 28871.
- U. C. Ugochukwu, M. D. Jones, I. M. Head, D. A. C. Manning and C. I. Fialips, *International Biodeterioration & Biodegradation*, 2014, 88, 185
- 55 21 R. Demir-Cakan, M. Morcrette, F. Nouar, C. Davoisne, T. Devic, D. Gonbeau, R. Dominko, C. Serre, G. Ferey and J. M. Tarascon, *Journal of the American Chemical Society*, 2011, 133, 16154.
 - 22 B. Guo, T. Ben, Z. Bi, G. M. Veith, X. G. Sun, S. Qiu and S. Dai, Chem Commun 2013, 49, 4905.
- 60 23 G. He, X. Ji and L. Nazar, Energy & Environmental Science, 2011, 4, 2878.
 - 24 Y. Fu and A. Manthiram, The Journal of Physical Chemistry C, 2012, 116, 8910.
- 25 Y. V. Mikhaylik and J. R. Akridge, *Journal of The Electrochemical Society*, 2004, **151**, A1969.